Molecular Catalysis 509 (2021) 111610

Contents lists available at ScienceDirect

Molecular Catalysis

journal homepage: www.journals.elsevier.com/molecular-catalysis

Stabilizing effect of α-Cr_2O_3 on highly active phases and catalytic performance of a chromium alumina catalyst in the process of isobutane dehydrogenation

S.R. Egorova *, R.R. Tuktarov, A.V. Boretskaya, A.I. Laskin, R.N. Gizyatullov, A.A. Lamberov

Alexander Butlerov Institute of Chemistry, Kazan Federal University, Kazan, 420008, Russia

ARTICLE INFO

Keywords:
Isobutane dehydrogenation
CrO_x/Al_2O_3 catalyst
α-Cr_2O_3
Amorphous Cr_2O_3
Chromium particles

ABSTRACT

The demand for C_3-C_5 olefins is constantly growing, that is why it is important to improve the performance of catalysts for dehydrogenation of light alkanes. The study regards the influence of the supports porous system, the contribution of α-Cr_2O_3 particles to the state of the active phase and the catalytic performance of the chromia-alumina catalysts in the isobutane dehydrogenation reaction. The catalysts were synthesized by impregnating the support with chromic acid. The supports and the catalysts were studied by the following techniques: low-temperature nitrogen adsorption, temperature-programmed desorption and reduction; UV-Vis- and Raman-spectroscopy, X-ray phase and X-ray fluorescence analyses. It was found that crystals of α-Cr_2O_3 are formed on a support with 56 m^2/g specific surface area and 7.1% (m/m) chromium content, that contributes to stabilization of the particles of highly active phases of amorphous Cr_2O_3 and polychromates and catalytic performance. Meanwhile, no α-Cr_2O_3 particles are formed on a support with a 103 m^2/g specific surface area and 7.4% (m/m) chromium content. Therefore, in the course of 54 regeneration reactions cycles, the rates of isobutylene formation and isobutylene selectivity are significantly reduced due to agglomeration of amorphous Cr_2O_3 particles, formation of di-, tri- chromates, and migration of part of chromium into the support structure.

1. Introduction

Non-oxidizing dehydrogenation of lower paraffins in the presence of chromium alumina catalysts (ChAC) is traditionally carried out to obtain the corresponding olefins used in the production of synthetic rubbers, fibers, films, plastics, high-octane fuel additives [1-3]. Growing number of areas of application of polymeric materials leads to a continuous increase in the consumption of olefin monomers. There are two types of processes for the dehydrogenation of lower paraffins on ChAC [2]. The FBD-4 process is designed to produce olefins under atmospheric pressure in a fluidized bed of microspherical catalyst with a granule size of 20-150 μm [3]. The Catadien/Catofin process is carried out under vacuum in adiabatic attached bed catalyst reactors for the production of diene hydrocarbons [2].

In case of the FBD-4 process, there is continuous circulation of microspherical ChAC in the reactor-regenerator system. The heat required for endothermic dehydrogenation is supplied to the reaction zone by a hot regenerated catalyst [4]. The catalyst is exposed to alternating high-temperature redox cycles of dehydrogenation (550-580°C) and regeneration (630-650°C) with large temperature drops and local overheating. γ-Al_2O_3 with a high heat capacity is used as a support to accumulate a large amount of heat during regeneration and to ensure an endothermic dehydrogenation process. A modern method of obtaining microspherical ChAC is impregnation of alumina supports with solutions of an active component, a promoter, and modifiers [5], which makes it possible to obtain an active and durable catalyst.

The properties of ChAC depend on the characteristics of the support, the active phase, and their interaction with each other. The activity in the reaction of paraffin dehydrogenation is determined by the distribution and oxidation state of chromium oxide compounds (oxides of Cr (III) and Cr (VI), chromates of alkaline promoter and aluminum), chromates of alkaline promoter and aluminum) on the catalyst surface. The state of the active component is affected by the concentration of chromium, alkaline promoter, the nature and content of the modifier, and the specific surface area of the catalyst. The nature and number of hydroxyl groups on the surface of the support affect the attachment and uniformity of distribution of the active component, and its porous system ensures transportation of reagent molecules to the active

* Corresponding author.
E-mail address: segorova@rambler.ru (S.R. Egorova).

https://doi.org/10.1016/j.mcat.2021.111610
Received 1 February 2021; Received in revised form 2 April 2021; Accepted 26 April 2021

component and the removal of reaction products.

Microspherical ChAC belongs to bifunctional catalytic systems involved in oxidation-reduction (target reaction of paraffin dehydrogenation) and acid catalysis (side processes of cracking and coke formation). The chromium alumina catalyst in the oxidized state contains Cr (III) and Cr(VI) oxide compounds [6]. Their relative contents depend on the structure of the support, the total amount of chromium, and the conditions of the catalyst thermal treatment [7]. Cr(III) ions are the active sites in dehydrogenation of lower paraffins [8-18].

At present, several types of Cr(III) and Cr(VI) ions are identified on the surface of fresh ChAC obtained after impregnation of the supports with a chromium-containing solution and thermal activation. Among them there are two types of Cr(VI) ions with the amount of 2-3% (m/m). The first one is of a grafted type, insoluble in water, chemically-bound with the surface of the alumina support and enters into aluminum chromates of various compositions [6]. The second one is of soluble type, enters into chromates of alkaline promoter and free chromium(VI) oxide. In a reducing medium, they are transformed into Cr_2O_3.

There are also several types of Cr(III) ions, including redox Cr(III) ions capable of oxidation to Cr(VI) or Cr(V) ions in a hydrocarbon medium, non-oxidation-reduction Cr(III) ions in amorphous Cr_2O_3 particles (Cr^{3+}_{aM}), α-Cr_2O_3 crystals (Cr^{3+}_{cryst}), $(Cr_xAl_{1-x})_2O_3$ solid solution, as well as in the form of so-called "isolated" particles [6, 19-22]. To ensure a high and stable activity, it is necessary to obtain a large number of coordination-unsaturated Cr(III) sites by forming highly dispersed Cr_2O_3 particles in ChAC. This may be achieved by applying an active component to a support with a developed specific surface area up to 100-150 m^2/g [23].

In the course of long-term operation, the ChAC activity and selectivity gradually decrease due to irreversible deactivation associated with changes in the state of the active component, which subsequently requires tightening the dehydrogenation conditions [5]. However, this does not allow a return to the catalytic performance of the fresh ChAC and, with a certain frequency, requires a complete replacement of the microspherical ChAC in a commercial reactor. To neutralize the effect of irreversible deactivation and to minimize the reduction in the production of olefins in a commercial reactor, it is customary to systematically partially unload the equilibrium catalyst and then add a fresh portion. As a result, a mixture of fresh and equilibrium ChAC circulates in the reactors, which does not allow to reliably estimate the reason for the decrease in the ChAC activity and selectivity [5].

Using the example of ChAC operated in reactors with an attached bed and oxidizing regeneration in the presence of water vapor, it is shown that irreversible deactivation is caused by a combination of factors: agglomeration of particles of Cr_2O_3 and Cr(VI) oxide compounds, gradual introduction of Cr(III) ions into the support structure with formation of chromium alumina spinel, and formation of α-Cr_2O_3 [19]. It is known that α-Cr_2O_3 is also formed at a chromium content of more than 11% or at a catalyst activation temperature above 900°C. In works [12, 13, 24] it was shown that α-Cr_2O_3 is inactive in dehydrogenation of lower paraffins. Therefore, it is better to reduce the chromium content in modern ChAC. In work [19], on the contrary, a high activity of α-Cr_2O_3 in the process of vacuum dehydrogenation of n-butane was established. The conflicting information requires the clarification of the effect of α-Cr_2O_3 particles and the value of the specific surface area of the support on the catalytic properties of ChAC of the fluidized bed, their contribution to deactivation during prolonged operation and oxidizing regeneration without the effect of water vapor.

As a result, the aim of the work is to study the effect of α-Cr_2O_3 and the parameters of the porous system of the aluminum oxide support on the catalytic performance of microspherical ChAC during long-term operation in the reaction of isobutane dehydrogenation with oxidative regeneration without water vapor. ChAC with similar chromium content was synthesized by impregnation with chromic acid of two industrial samples of supports with about 2 times difference in the specific surface area. The catalytic performance was compared for changes in the state of chromium oxide compounds in ChAC before and after reaction-regeneration cycles in a laboratory reactor at temperatures corresponding to the large-scale FBD-4 process.

2. Materials and methods

The study subject is microspherical aluminochromium catalysts for the dehydrogenation of isobutane to isobutylene with a granule size of 40-150 μm. For their synthesis, we used industrial alumina supports with the γ-Al_2O_3 structure, obtained through calcining at 550°C the microspherical boehmite supports (PJSC Nizhnekamskneftekhim, Nizhnekamsk city, Russia). The catalyst supports were synthesized according to the earlier developed technology of sequential thermal and hydrothermal treatment of aluminum trihydroxide in an autoclave at T = 180-190°C for 60 min. [25, 26]. ChAC was prepared by impregnating the supports with an aqueous solution of CrO_3 (analytical grade, GOST 3776-78, Russia) and potassium carbonate (analytical grade, GOST 4221-76, Russia), followed by vacuum drying. In an industrial vacuum mixer, an industrial ChAC (IC) was obtained, in a laboratory rotary-vacuum evaporator - a laboratory ChAC (LC) was obtained. A support was placed in a vacuum mixer and a rotary-vacuum evaporator, subjected to degassing. Then, at a residual pressure of 40 kPa, aqueous solutions of the precursors of the active component (chromic acid) and the promoter (potassium carbonate) were brought in in amounts corresponding to the moisture capacity of the support. After impregnation, the catalyst was dried in vacuum at a residual pressure of 10-20 kPa and then thermoactivated. Thermal activation of industrial ChAC was carried out in an industrial drum furnace at 750°C. Thermal activation of the laboratory catalyst was carried out in a muffle furnace at 750°C for 4 h (heating rate 4°C/ min).

Tests of ChAC in the reaction of isobutane dehydrogenation were carried out in two parallel working laboratory units with a fluidized bed, using tubular reactors (stainless steel AISI 304) with an inner diameter of 30 mm. In the lower part of the reactors, in order to uniformly distribute the gas along the diameter, a ceramic distribution grid with a hole diameter of 100-200 μm and a free section fraction of 30% was installed. The volume of ChAC loaded into the first reactor was 100 cm^3, in the second - 150 cm^3, the volumetric flow rate of isobutane was 400 h^{-1}, and the reaction temperature was 570°C. In the course of the reaction, temperature drops in the ChAC layer did not exceed 2°C. The dehydrogenation cycle consisted of dehydrogenation operations for 40 min, nitrogen purge for 5 min, regeneration with air at 650°C for 30 min, and nitrogen purge for 5 min. Then the cycle was repeated. During the dehydrogenation, samples of the contact gas were taken in 20 and 40 min. ChAC testing was carried out continuously within 54 cycles. Catalyst samples were taken from both reactors every 9 cycles. A sample from the first reactor was sent for analysis of physicochemical properties. A sample from the second reactor of the same mass was placed in the first reactor instead of the sample taken.

The flow rates of the isobutane fraction (99,97 wt.% i-C_4H_{10}, 0,03 wt.% i-C_4H_8), argon (purity 99.99 %), and air were set using electronic gas flow controllers with the help of a computer. Before entering the gas flow regulator, the isobutane fraction, argon, hydrogen (purity 99.99 %), nitrogen (purity 99.99 %), and air were dried using calcium chloride and NaX zeolite. The temperature in the catalyst bed was controlled using a chromel-alumel thermocouple, maintaining the set value with an RPN-4 thermostat (ITM, Russia), also controlled from a computer. The accuracy of maintaining the temperature is 1°C.

The composition of the isobutane fraction and the contact gas was analyzed by an on-line gas chromatography. The composition of hydrocarbons was monitored on a GKh-1000 chromatograph (Khromos, Russia) with a flame ionization detector. A VP-Alumina/KCl capillary column (VICI Valco, USA) was used. Components were identified by calibrating the chromatograph with reference substances. The relative error in determining the concentrations of the components was no more than 10%. The content of H_2, CH_4 was determined on a GKh-1000

chromatograph (Khromos, Russia) with a thermal conductivity detector using a column with NaX. The relative error in determining the concentrations of the components was no more than 10%.

According to the results of chromatographic analysis, the conversion of isobutane (X) and the selectivity to isobutylene were calculated using the formula

$$S = \frac{C^{\text{cont.gas}}_{i-C_4H_8} - C^{\text{feedstock}}_{i-C_4H_8}}{C^{\text{feedstock}}_{i-C_4H_{10}} - C^{\text{cont.gas}}_{i-C_4H_{10}}} \times 100, \ \%$$

where $C^{\text{cont.gas}}_{i-C_4H_8}$ is the isobutylene concentration in the contact gas,% (m/m); $C^{\text{feedstock}}_{i-C_4H_8}$ is the isobutylene concentration in the feedstock, % (m/m); $C^{\text{feedstock}}_{i-C_4H_{10}}$ is the isobutane concentration in the feedsctock, % (m/m); $C^{\text{cont.gas}}_{i-C_4H_{10}}$ is the isobutane concentration in the contact gas, % (m/m).

The selectivity defined as the yield of isobutylene per decomposed isobutane. No adverse reactions associated with the thermal transformation of isobutane or isobutylene in the gas phase were observed in our experiment.

The specific rate of isobutylene formation was taken as the catalyst activity, which was calculated by the formula

$$r = \frac{\omega_{i-C_4H_8}}{C_{\text{Cr}}}, \text{mol } i-C_4H_8 \cdot \text{mol } Cr^{-1} \cdot \text{ч}^{-1}$$

where ω_{i-C4H8} is isobutylene yield, mol $iC_4H_8 \cdot h^{-1}$

C_{Cr} is concentration of chromium in the catalyst, mol

The content of chromium and potassium was analyzed on a Clever C31 X-ray fluorescence spectrometer (Eleran, Russia). Samples for elemental analysis were prepared by grinding the samples in a planetary mill and pressing into tablets. X-ray fluorescence spectra were recorded in vacuum using a rhodium tube as a radiation source. The scanning area of the sample was 1 cm^2.

The carbon content in the catalysts was determined on a HORIBA EMIA-510 device (Japan) with an IR detector for CO_2 according to the ASTM method [27] by burning a catalyst sample in an oxygen flow of ~ 1 g at a temperature of 1450 °C for 60 s.

To determine the Cr(VI) content, a solution of sulfuric acid and sodium pyrophosphate was added to the catalyst sample (0.4-0.6 g) under stirring. Then a solution of potassium iodide was added and allowed it to stand in the dark for 5 min. To determine the content of soluble Cr(VI), the aqueous extracts of ChAC samples were analyzed in a similar way. The concentration of bound Cr(VI) was determined as the difference between the total and soluble Cr(VI).

X-ray phase analysis was performed on a MiniFlex 600 diffractometer (Rigaku, Japan) with a D/teX Ultra detector using long-wave CuK radiation (40 kV, 15 mA) in the 2θ range from 5 to 100 ° with a step of 0.02° and an exposure time at each point of 0.24 s. The phases were identified in accordance with the PDF Powder Standards Database (JCPDS). The sizes of coherent scattering regions (CSR) of α-Cr_2O_3 were calculated using the Selyakov-Scherer formula. The error in determining the size of CSR is about 10%.

The specific surface area (S_{sp}) and pore volume (V_p) were measured by nitrogen adsorption-desorption on a universal analyzer Autosorb iQ MP 2400 (Quantachrome, USA). The specific surface area was calculated with basis on the surface area of the nitrogen molecule of 0.162 nm^2 and the density of N_2 in the normal liquid state of 0.808 g/cm. The S_{sp} measurement accuracy was 3%. Adsorption isotherms were obtained at –196 °C after degassing the sample at 500 °C to a residual pressure of 0.013 Pa. Calculations of the porosimetric volume and the pore volume distribution by diameter were performed along the desorption branch of the isotherm using the standard Barrett – Joyner – Highland procedure. Measurement accuracy is 5%.

UV-visible diffuse reflectance spectra were obtained on a V-650 scanning two-beam spectrophotometer (Jasco, Japan) connected to an ISV-722 integrating sphere (Jasco, Japan) with a diameter of 60 mm, coated from the inside with $BaSO_4$. A $BaSO_4$ plate was used as a standard. To record the spectra, samples of ChAC and α-Cr_2O_3, 40-100 μm in size, were placed in a holder with a quartz window. The spectra were recorded in the range of 200-800 nm (12500-50000 cm^{-1}) with a spectral resolution of 2 nm. The data on the diffuse reflection of samples in the UV-visible region are presented as the dependence of the Kubelka-Munk function on the wave number. The UV-visible spectra of the AChC and α-Cr_2O_3 samples were decomposed into Gaussian components to determine the position and intensity of the absorption band (a.b.) maxima .

Raman scattering spectra were obtained on an inVia Qontor dispersive microspectrophotometer (Renishaw, Great Britain) with a diffraction grating of 1800 pcs/mm with a Leica DM2700 M microscope and an Nd:YAG laser (radiation wavelength is 532 nm). We calibrated the spectral lines and the position of the laser beam on a single-crystal silicon standard. The diameter of the focused laser spot on the sample is ~ 1 μm. The laser power on the sample did not exceed 10 mV. The spectra were recorded in the range of shifts of 100-1100 cm^{-1} with a spectral resolution of 2 cm^{-1}. Each spectrum was obtained by averaging 10 exposures of 30 seconds each.

The surface acidity of the supports and ChAC was analyzed by temperature-programmed desorption of ammonia (NH_3-TPD) on a flow-through instrument with a ChemBet Pulsar thermal conductivity detector (Quantachrome, USA). The stage of adsorption was carried out in an ammonia flow for 30 min at a temperature of 100°C. After adsorption, the physically adsorbed ammonia air stripping with helium at 100°C for 30 min was carried out. Then, the sample was cooled to room temperature in a helium flow. Temperature-programmed desorption was carried out from room temperature to 700°C at a rate of 10°C/min. Calculations of the NH_3-TPD data on the distribution of acid sites ($N_{a.s.}$) were carried out according to the method described in [28].

The study of ChAC by the method of temperature-programmed hydrogen reduction (H_2-TPR) was carried out on a flow-through device with a ChemBet Pulsar thermal conductivity detector (Quantachrome, USA). Before reduction, the catalyst was kept in a flow of a gas mixture of 5% vol. oxygen in nitrogen at 650°C for 60 min. Then, it was cooled to room temperature in a flow of helium. Temperature-programmed desorption was carried out from room temperature to 700°C at a rate of 10°C/min.

Chemisorption titration of chromium with oxygen was performed on an AutoChem 2950 HP instrument (Micromeritics). The samples were oxidized in a quartz reactor for 2 h at 500°C in an oxygen flow. Reduction was carried out at 500°C in a flow of hydrogen for 2 h. After cooling in a flow of helium to -78°C, the sample was titrated with oxygen by the pulsed method (25 ml O_2/min) until complete saturation. From the data obtained, the surface area of chromium and the average size of its particles were calculated.

3. Results

3.1. Catalytic tests

Fig. 1 shows the main catalytic indicators of laboratory and industrial ChAC obtained at 20 and 40 minutes of cycles. Based on the results of our preliminary tests, the development of catalysts is completed by 20 minutes and their maximum activity is achieved. 40 minutes is the average residence time of an individual microspherical catalyst pellet in the reaction zone in a commercial reactor. During the first nine cycles, laboratory and industrial ChAC are characterized by equal (56.5-57.6 %) isobutane conversion. At the same time, laboratory ChAC is more selective. Their selectivity for isobutylene is 88.8-89.4 % versus 85.8-87.4 % for industrial ChAC. In the contact gas obtained at the laboratory ChAC, fewer cracking products (C_1-C_3 hydrocarbons) are identified, and fewer carboceous deposits are formed on the surface of carbonized samples. The carbon content in the samples taken after 40 minutes of each cycle is 1.6-1.7 times lower than in the samples of the industrial ChAC (Fig. 2). For both ChACs, by 40 minutes compared to 20 minutes, a

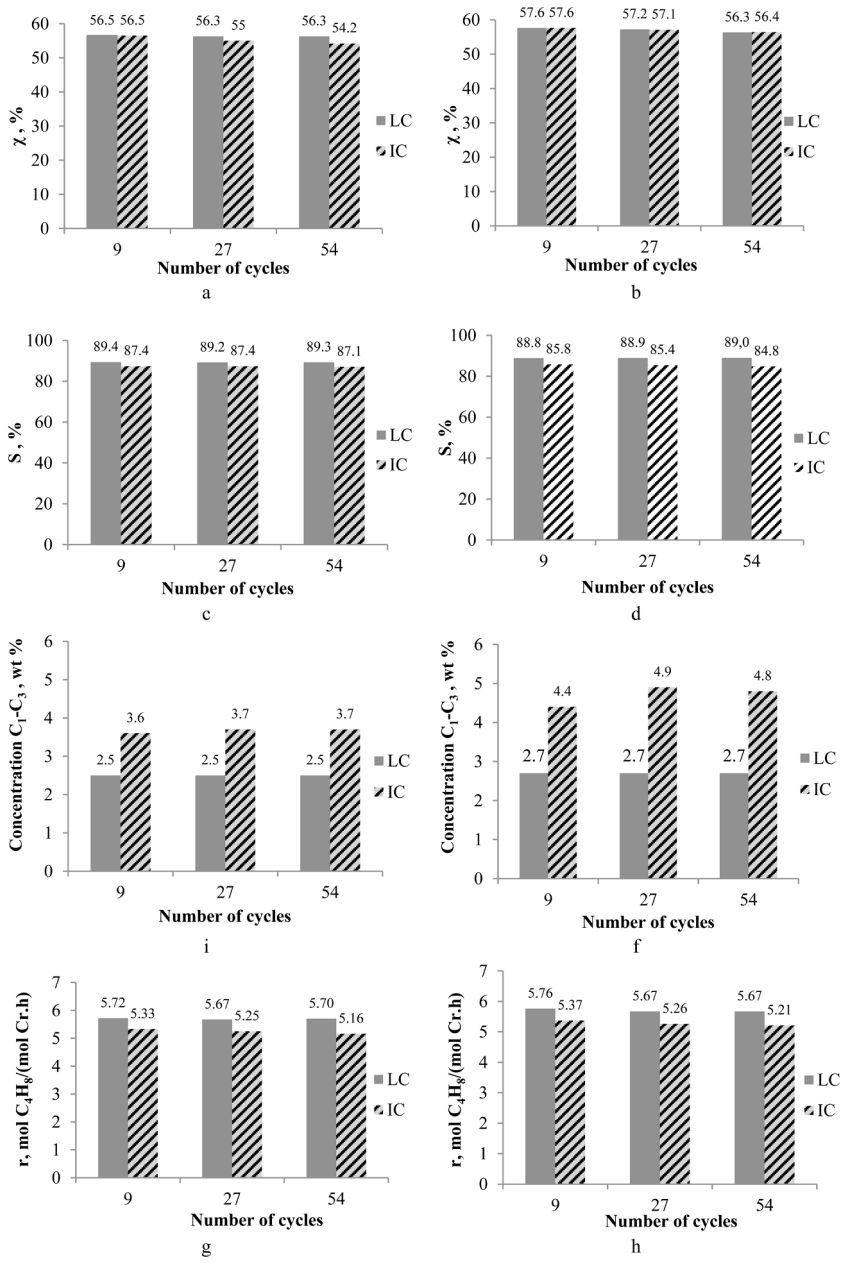

Fig. 1. Catalytic performance at 20 minutes (a, c, i, g) and 40 minutes (b, d, f, h) of reaction: laboratory sample (LC), industrial sample (IS)

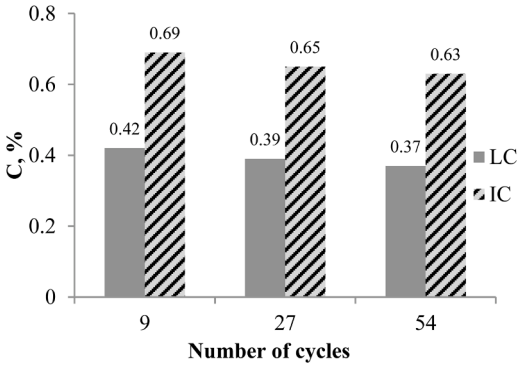

Fig. 2. Carbon concentration in catalysts

slight increase in the conversion and rate of isobutylene formation with a decrease in the selectivity to isobutylene, due to an increase in the yield of C_1-C_3 hydrocarbons, is noted. This trend persisted throughout all 54 test cycles. Moreover, a decrease in the conversion of isobutane and the rate of isobutylene formation by 0.1-1.3% and 0.02-0.09 mol iC_4H_8·Моль Cr^{-1}·h^{-1}, respectively, with almost unchanged selectivity for isobutylene, is noted on the laboratory ChaC. Whereas on the industrial ChAC, the conversion of isobutane and the rate of isobutylene formation decrease by 1.2-2.3 % and 0.16-0.17 mol iC_4H_8·mol Cr^{-1}·h^{-1}, respectively, and the selectivity for isobutylene is changing by 0.3 -1.0%.

3.2. *X-ray phase analysis*

On the diffraction pattern of fresh and used in 54 cycles of laboratory ChAC samples (Fig. 2, curves 1 and 2), the diffraction lines of the γ-Al_2O_3 support and the α-Cr_2O_3 active component are identified. The α-Cr_2O_3 concentration, determined through the external standard method, in

Table 1
Content and surface concentrations of chromium oxide compounds in ChAC samples

Types of chromium oxide compounds	Chromium content (% wt) and its surface concentration (at_{Cr} / nm^2)			
	Laboratory ChAC		Industrial ChAC	
	Fresh	After cycle 54	Fresh	After cycle 54
Cr_2O_3 and chromates	7,1 (20,1)	7,5 (21,6)	7,4 (9,9)	7,5 (11,6)
α-Cr_2O_3	3,6 (10,2)	3,5 (10,1)	-	-
Amorphous Cr_2O_3	2,8 (7,8)	3,0 (8,7)	5,6 (7,5)	5,7 (8,8)
Chromates	0,7 (2,1)	1,0 (2,8)	1,8 (2,4)	1,8 (2,8)
Grafted form	0,2 (0,6)	0,2 (0,7)	0,5 (0,6)	0,5 (0,8)
Soluble form	0,5 (1,5)	0,7 (2,1)	1,3 (1,7)	1,3 (2,0)

fresh and used samples was 5%. The CSR sizes of α-Cr_2O_3 particles calculated for the plane (012) in fresh ChAC were 18 nm. After 54 cycles, the diffraction pattern of the catalyst remains almost unchanged. The intensity of the diffraction lines of α-Cr_2O_3 is somewhat reduced, which indicates the partial amorphization of its particles during numerous redox cycles. The CSR sizes of α-Cr_2O_3 particles increase to 22 nm. It can be assumed that the smallest α-Cr_2O_3 particles undergo amorphization.

On the diffraction patterns of fresh and used in 54 cycles industrial ChAC samples (Fig. 2, curves 3 and 4), only the diffraction lines of the γ-Al_2O_3 support are identified. After 54 cycles, the diffraction pattern of the catalyst does not change.

3.3. Elemental and chemical analysis

In fresh laboratory and industrial ChAC, the total chromium content was 7.1 and 7.4 %, respectively, and potassium - 1.0 and 1.7 %, respectively. Such concentrations were selected on the basis of preliminary optimization of the chemical composition of ChAC on these supports, which provided the best activity and selectivity performance of the samples. After 54 test cycles, the chromium content in both catalysts was 7.5%. The potassium content did not change.

The content of various forms of oxides of Cr (III) and chromates in fresh and obtained after 54 test cycles of ChAC (after oxidizing regeneration) are shown in Table 1. In the laboratory ChAC, the proportion of chromium in the composition of amorphous Cr_2O_3 is 39-40 % of the total amount. Moreover, the proportion of chromium, which is a part of chromates, in the process of testing increases due to their soluble form from 10 to 13% of the total amount of chromium. In industrial ChAC, the proportion of chromium, which is part of both forms of chromates, is 24 % of the total amount of chromium and does not change over 54 cycles.

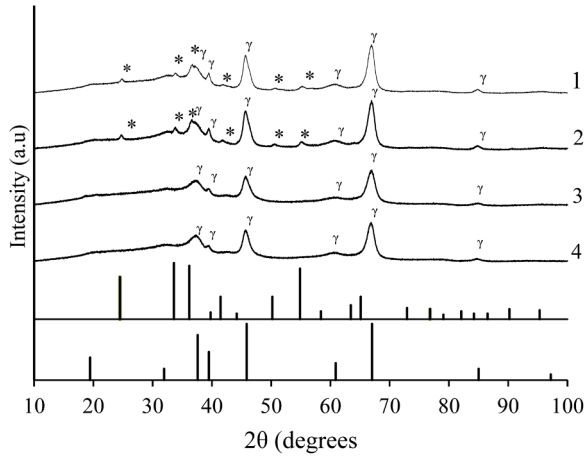

Fig. 3. Diffractograms: LC (1), LC-54 cycles (2), IC (3), IC – 54 cycles (4), (5) a - Cr_2O_3 ICDD (PDF-2 Release 2014 RDB) 01-078-5450, (6) γ - Al_2O_3 ICDD (PDF-2 Release 2014 RDB) 00-010-0425

3.4. Texture analysis

The textural characteristics of the support samples, as well as laboratory and industrial ChAC, are shown in Fig. 3 and in Table 2. The introduction of chromium reduces the specific surface area and pore volume of the catalysts by a factor of 1.2-1.4 compared to the initial supports. Surface chromium compounds are predominantly distributed in pores with a diameter of 5-20 nm, the volume of which decreases from 0.13 to 0.08 cm^3/g for laboratory ChAC and from 0.29 to 0.20 cm^3/g for industrial ChAC.

The specific surface area and pore volume of the laboratory ChAC are 41 m^2/g and 0.18 cm^3/g, respectively. On the differential curve of the pore volume distribution according to pore diameters, two pronounced maxima are identified: an intense narrow one at D_p = 4 nm, and an intense one at D_p~15nm broadening to D_p=25 nm. In the course of the isobutane dehydrogenation, at each cycle, carbonaceous deposits accumulate in the catalyst mainly in the region of pore diameters less than 10 nm. Carbonaceous deposits are finely porous, as the surface area and pore volume increase simultaneously. After oxidizing regeneration, the surface area is reduced by 4 m^2 g, which is due to the fixation of

Table 2
Textural characteristics of supports, fresh and spent in the process of dehydrogenation of isobutane ChAC

Sample	S_{sp}, m^2/g	V_p, cm^3/g	D_p, nm	Pore volume distribution (cm^3/g) over pore diameters		
				<5 nm	5-20 nm	> 20 nm
			Laboratory ChAC			
Catalyst support γ-Al_2O_3	56	0,25	19	0,03	0,13	0,09
Fresh catalyst	41	0,18	18	0,02	0,08	0,08
Carbonized after cycle 9	41	0,18	18	0,02	0,07	0,09
Carbonized after cycle 27	49	0,21	16	0,03	0,09	0,09
Carbonized after cycle 54	59	0,21	14	0,05	0,09	0,07
Oxidative regeneration after cycle 54	40	0,18	19	0,02	0,07	0,09
			Industrial ChAC			
Catalyst support γ-Al_2O_3	103	0,31	12	0,02	0,29	0,04
Fresh catalyst	86	0,26	12	0,02	0,20	0,04
Carbonized after cycle 9	80	0,27	13	0,02	0,21	0,04
Carbonized after cycle 27	67	0,25	15	0,01	0,20	0,04
Carbonized after cycle 54	64	0,23	14	0,02	0,17	0,04
Oxidative regeneration after cycle 54	75	0,27	14	0,02	0,20	0,05

Table 3
Ammonia TPD data

Sample	$\Sigma N_{a.s.}$, μmol NH_3/g	Distribution of $N_{a.s.}$, μmol NH_3/g		
		E_{des} <100 kJ/mol	100< E_{des} <130 kJ/mol	E_{des} >130 kJ/mol
		Laboratory ChAC		
Catalyst support	73	24	41	8
Fresh catalyst	19	9	10	-
After cycle 54	33	8	24	1
		Industrial ChAC		
Catalyst support	209	14	127	68
Fresh catalyst	67	12	53	2
After cycle 54	89	13	69	7

unburned carbon deposits in fine pores with a diameter of less than 5 nm and partially in pores with a diameter of 5-10 nm. The residual carbon content in the catalyst does not exceed 0.020 % (m/m), and the total pore volume corresponds with a fresh sample.

The specific surface area and pore volume of industrial ChAC are 86 m^2/g and 0.26 cm^3/g, respectively. The differential curve of the pore volume distribution according to diameters also contains two pronounced maxima: a narrow one at $D_p = 4$ nm, and also more intense at $D_p = 9$ nm, broadening to $D_p = 15$ nm. From cycle to cycle, the porous catalyst system is transformed. The second maximum on the differential curve shifts to the region of large diameters up to 10 nm and broadens to $D_p = 25$ nm. In this case, the average pore diameter increases from 12 to 14 nm. In the course of reaction, carbonaceous deposits are formed mainly in the area of pore diameters less than 15 nm. By the end of the tests, after oxidizing regeneration, carbon deposits remain only in fine pores with a diameter of less than 5 nm, and the rest of the pores are completely freed. The residual carbon content is 0.015 % (m/m). As a result, after 54 cycles, a significant (by 11 m^2/g) reduction in the specific surface area is noted in the regenerated sample due to the disappearance of a part of the pores in the range of diameters of 5-10 nm. The total pore volume increases to 0.27 cm^3 g.

3.5. Temperature-programmed ammonia desorption analysis

The properties of the support determine the nature and concentration of surface hydroxyl groups formed on its surface, the number of coordination-unsaturated aluminum atoms. They determines the acidic properties of the surface of alumina supports and ChAC, which were studied by the NH_3-TPD (Table 3). The strength of the sites was estimated from the ammonia desorption temperature corresponding to a certain desorption activation energy (E_{des}). Acid sites are taken as weak, the activation energy of which is less than 100 kJ/mol, the medium strength is 100-130 kJ/mol, and the strong ones are more than 130 kJ/mol.

The total concentration of surface acid sites of laboratory ChAC is 73 μmol of NH_3/g. The velocity profile of ammonia desorption versus temperature is observed in the range of 76-398 °C with a desorption peak at 156 °C and a low-intensity shoulder in the range of 243-398 °C. The share of the strongest acid sites is 11%. In contrast to the laboratory sample, the velocity profile of the ammonia desorption of industrial ChAC is observed in a wider temperature range from 94 to 502 °C with desorption peaks at 180 and 236 °C. The total concentration of acid sites is 209 μmol of NH_3/g. At the same time, the concentration of strong sites is 10 times higher, of medium sites is 3 times higher, and of weak centers, on the contrary, is almost 2 times lower.

Chromium oxide compounds and potassium oxide reduce the surface acidity of fresh laboratory and industrial ChAC by 3.8 and 3.1 times, respectively. In the first case, the velocity profile of the ammonia desorption narrows to 60-270 °C, and the desorption peak shifts to 140 °C. At the same time, the concentration of all types of acid sites decreases and the strongest ones disappear. After 54 cycles of operation, the total concentration of acid sites increases from 19 to 33 μmol of NH_3/g, mainly due to sites of medium strength. Corresponding changes are also noted for industrial ChAC - the velocity profile of the ammonia desorption is noted in the range of 100-360 °C with a desorption peak at 155 °C. By the end of the tests, the surface concentration of strong and medium-strength sites grows, which increases the total acidity from 67 to 89 μmol of NH_3/g.

3.6. Diffuse reflectance spectroscopy analysis

Fig. 4 shows the UV-vis spectra of oxidized and reduced forms of fresh and used in 54 cycles ChAC. All spectra are typical for oxides of Cr (III) and chromates distributed over the surface of alumina. The absorption bands related to the octahedral $Cr(III)_{oct}$ ion of the non-oxidation-reduction type in Cr_2O_3 and the Cr(VI) ion in chromates are identified . In the visible region of the spectrum, there are absorption bands associated with the electronic d–d junction in the octahedral Cr

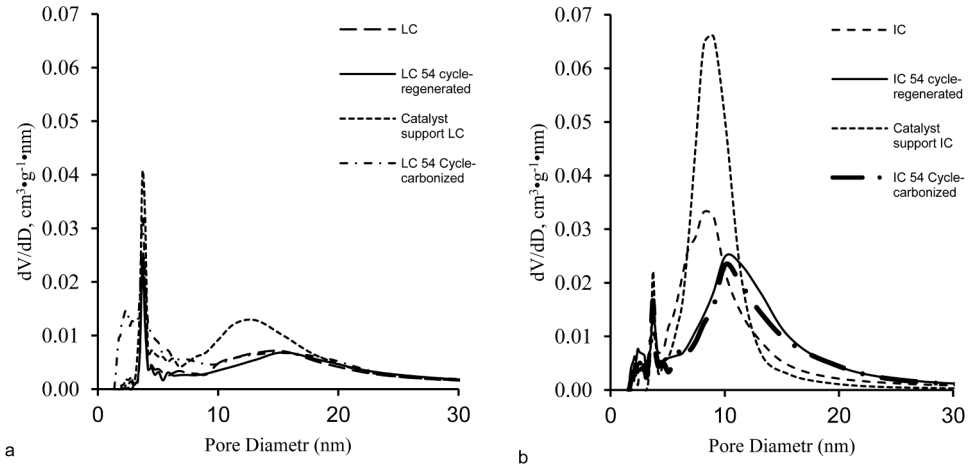

Fig. 4. Differential curves of pore volume distribution over pore diameters: laboratory sample (a); industrial sample (b)

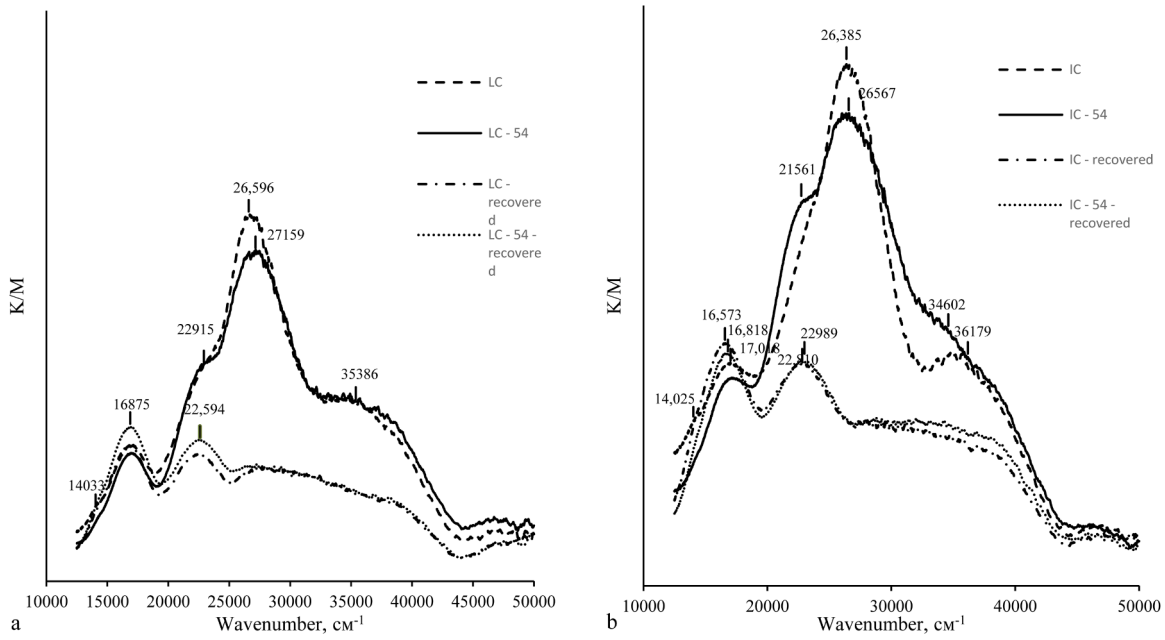

Fig. 5. UV-Vis diffuse reflectance spectra: laboratory sample (a); industrial sample (b)

$(III)_{oct}$. A weak shoulder at 14030 cm^{-1} arises due to the $^4A_{2g}\rightarrow{}^4E_g$ magnetic dipole transition. According to [29] the spin ban is lifted as a result of vibronic interaction. These absorption bands can be identified in amorphous Cr_2O_3 [38]. The bands at 16700-17000 cm^{-1} correspond to the electronic d-d junction $^4A_{2g}\rightarrow{}^4T_{2g}$ in the octahedral $Cr(III)_{oct}$ ion, and at 21600-23000 cm^{-1} they refer to the complex signal characteristic of the Cr(III) and Cr(VI) ions corresponding to the electronic d-d junction $^4A_{2g}\rightarrow{}^4T_{1g}$ in the octahedral $Cr(III)_{oct}$ ion, as well as to the O^2-Cr(VI) charge transfer in chromates [30]. Both signals are characteristic of amorphous Cr_2O_3 and crystalline α-Cr_2O_3 particles. In the UV spectrum, there are also intense absorption bands associated with the charge transfer of O^2-Cr (VI) in chromates. The signal at 21600 cm^{-1} is related to the presence of chromates, at 26400-27200 cm^{-1} – to monochromates and at 34600-35400 cm^{-1} – to di-, tri- and polychromates.

In the spectrum of the oxidized form of fresh laboratory ChAC, a shift of 200 cm^{-1} towards the region of high frequencies of absorption bands at 16875 cm^{-1} relative to that in the spectrum of α-Cr_2O_3 indicates the effect of γ-Al_2O_3 crystal field on the energy of the d-d junction in the Cr $(III)_{oct}$ ion as a result of the incorporation of some chromium ions into the crystal lattice of the alumina support. After 54 cycles of regeneration reactions in the visible spectrum of the oxidized sample, there are no significant changes, but in the UV region, a shift in the absorption band is noted at 26596 cm^{-1} to 27159 cm^{-1} with simultaneous broadening into the region of large wavenumbers of the a.b. at 35386 cm^{-1}, which indicates a decrease in the proportion of monochromates and their polymerization. In turn, the absorption bands in the spectra of the reduced samples slightly increase at 14033, 16875 and 22594 cm^{-1}, which may be a consequence of the appearance of additional redox Cr (III) in the composition of amorphous Cr_2O_3.

The spectrum of the oxidized form of fresh industrial ChAC is close to the spectrum of the laboratory sample. A smaller shift (by 151 cm^{-1}) toward higher frequencies of a.b. at 16818 cm^{-1} relative to that in the spectrum of α-Cr_2O_3 indicates a smaller amount of introduced Cr(III) ions into the crystal lattice of the alumina support. After 54 cycles of reactions-regenerations in the visible spectrum, the intensity of absorption bands noticeably decreases at 14025 cm^{-1}, which probably indicates a decrease in the fraction of amorphous Cr_2O_3 due to the incorporation of a part of Cr(III) into the structure of the alumina support, since the a.b. is shifted simultaneously at 16818 cm^{-1} in the region of high frequencies up to 17018 cm^{-1}. In the UV- spectrum, in contrast to a decrease in the intensity of the a.b. at 26385 cm^{-1} and its displacement up to 27159 cm^{-1}, the intensities of the absorption bands significantly increase at 21516 and 36179 cm^{-1}. The latter shifts to the region of lower energies up to 34602 cm^{-1}. Taken together, this indicates a decrease in the proportion of monochromates in favor of di- and trichromates, which, after reduction to amorphous Cr_2O_3, may be found in the spectra of the reduced samples by an increase in the a.b. at 22989 cm^{-1}.

3.7. Raman spectroscopy analysis

The nature of Cr(VI) compounds was studied in more detail by Raman spectroscopy. Fig. 5 shows the Raman spectra of oxidized forms of fresh and used in 54 cycles of catalysts in the region of vibrations of Cr-O bonds in chromates at Raman shifts from 700 to 1100 cm^{-1}.

In fresh laboratory ChAC, the bulk of Cr(VI) compounds is stabilized in the form of mono- and polychromates. The Raman spectrum identifies signals at 854–890, 940 and 1040 cm^{-1}, corresponding to vibrations of Cr–O bonds in dehydrated polychromates, hydrated di-trichromates, and dehydrated monochromates, respectively [17, 31-35]. After 54 cycles, the absorption bands intensify in the spectrum of the reoxidized sample at 850-885 and 940 cm^{-1}, the intensity of the a.b. decreases at 1040 cm^{-1}, which indicates the transformation of some of the monochromates into di-, tri- and polychromates.

In fresh industrial ChAC, similar Cr(VI) compounds are formed, but in larger quantities. In the Raman spectrum of the intensity the a.b. at 846-865, 900 and 1020 cm^{-1} 2-2.5 times higher than in the spectrum of a laboratory catalyst. After 54 cycles in the spectrum of the reoxidized sample, the intensity of a.b. significantly decreases at 849 cm^{-1}, the intensity of the band at 890 cm^{-1} increases, the band at 1020 cm^{-1} disappears. A new intense band appears at 940 cm^{-1}, corresponding to vibrations of Cr-O bonds in hydrated di- and trichromates.

3.8. Temperature-programmed hydrogen reduction

H_2 TPR profiles of the reduced forms of fresh and used in 54 cycles of regeneration reactions of ChAC samples are shown in Fig. 7. The H_2 TPR profile of fresh laboratory ChAC contains a signal of hydrogen absorption in the range of 350-580 °C. Decomposition of the profile into Gaussian components gives two subcomponents. The first includes two

high-intensity maxima at 434 and 455 °C, the second includes low-intensity maxima at 501 and 529 °C. The former correspond to the easier reduction of polychromates mainly. The latter correspond to the hindered reduction of chromate anions stabilized by the support surface, with the formation of "isolated" mono-, di- and tri-chromates strongly bound to the Al(III) ion. The content of Cr(VI), stabilized on the surface, in terms of CrO_3 for the fresh catalyst was 0.29 % (m/m). The calculation was carried out on the basis of the reaction equation $2CrO_3 + 3H_2 \rightarrow Cr_2O_3 + H_2O$ (based on the amount of the absorbed hydrogen). After 54 cycles of regeneration reactions, the content of Cr(VI) in terms of CrO_3 decreased slightly to 0.27% (m/m). But, at the same time, there is a shift in the effect of reduction of surface Cr(VI) oxide compounds to lower temperatures. A new signal appears at 417°C, and the signal at 434°C almost halves the intensity due to a decrease in the proportion of monochromates and the formation of additional polychromates. A new peak identified in the high-temperature region at 568°C indicates the formation of a small amount of a new, most difficult-to-reduce form of Cr (VI) oxide compounds, which is probably not involved in the Cr(III)↔Cr (VI) redox process.

The H_2 TPR profile of a fresh commercial ChAC contains only one signal of hydrogen absorption at 428 °C. The calculated content of Cr (VI) in terms of CrO_3 was 0.64 % (m/m). After 54 cycles of regeneration reactions, the content of Cr(VI) 1.3 times decreased. In this case, the effect of Cr(VI) reduction on the TPR profile shifts to the high-temperature region up to 434 °C with the appearance of an additional high-temperature component, the decomposition of which into Gaussian components gives effects at 473 and 568 °C, which also indicates the formation of less active and difficult to restore CrO_3 forms.

Table 4
Results of chemisorption titration of chromium with oxygen

Sample	Average particle diameter of chromium, nm	Chromium surface area, m^2/g
LC	582	1,9
LC - 54	570	2,0
IC	304	3,8
IC - 54	335	3,4

3.9. Oxygen chemisorption analysis

The results of chemisorption titration of chromium in the samples are presented in Table 4. The size of chromium particles in fresh laboratory ChAC is 582 nm and after 54 reaction-regeneration cycles decreases to 570 nm, while the chromium surface area changes from 1.90 to 2.02 m^2/g. The sizes of chromium particles in industrial ChAC are approximately 1.9 times less than in laboratory ones, and during operation they increase, which is accompanied by a reduction in their surface from 3.8 to 3.4 m^2/g.

4. Discussion

Table 1 shows data on the distribution of chromium in the composition of its various oxides and chromates in fresh and used samples of ChAC. The catalysts differ significantly in the values of the surface chromium concentrations (at_{Cr}/nm^2). In a laboratory sample synthesized using a support with a 2.0 and 2.8 times lower specific surface area (Table 2) and the number of acid sites (Table 3), respectively, the surface concentration of chromium is 2 times higher. As it is known, with a small amount of terminal Al-OH groups, CrO_3 deposited from a solution of chromic acid is distributed on the surface in a physically adsorbed state. After thermal activation is transformed into crystalline α-Cr_2O_3. In turn, the surface polychromates of aluminum and potassium (a soluble form of chromates) obtained by the interaction of Al-OH groups with CrO_4^{2-} or $Cr_2O_7^{2-}$ ions through the substitution of the OH^- anion form predominantly amorphous Cr_2O_3 after thermal activation. Through the strong interaction with the surface of the alumina support, thermally stable mono-, di-, and trichromates of aluminum (grafted form) are also formed. Mono-, di-, tri- and polychromates according to UV-vis and Raman spectroscopy are formed in different ratios in laboratory and industrial ChAC (Fig. 5, 6).

In the laboratory ChAC, the high surface concentration of chromium is provided precisely by α-Cr_2O_3, the contribution of which reaches 51%. Excluding chromium included in the composition of chromates, the contribution of amorphous Cr_2O_3 to the surface concentration of chromium decreases to 39% in a fresh sample and 40% after 54 test cycles. In the industrial ChAC it is much higher and amounts to 76%. For both of ChAC at the beginning of the tests, the calculated total surface chromium concentrations related to amorphous Cr_2O_3 and both forms of

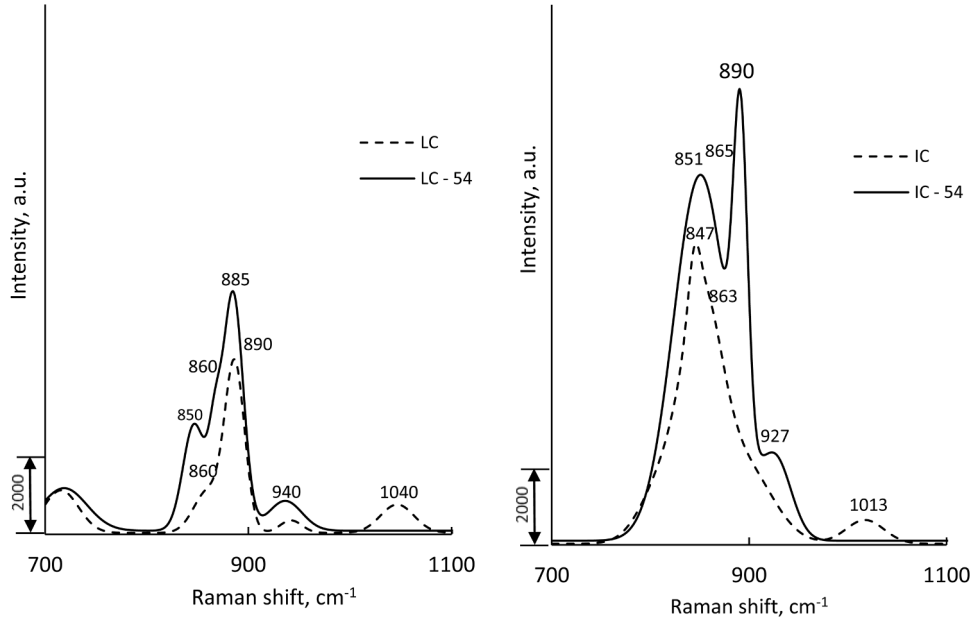

Fig. 6. Raman spectrs: laboratory sample (a); industrial sample (b)

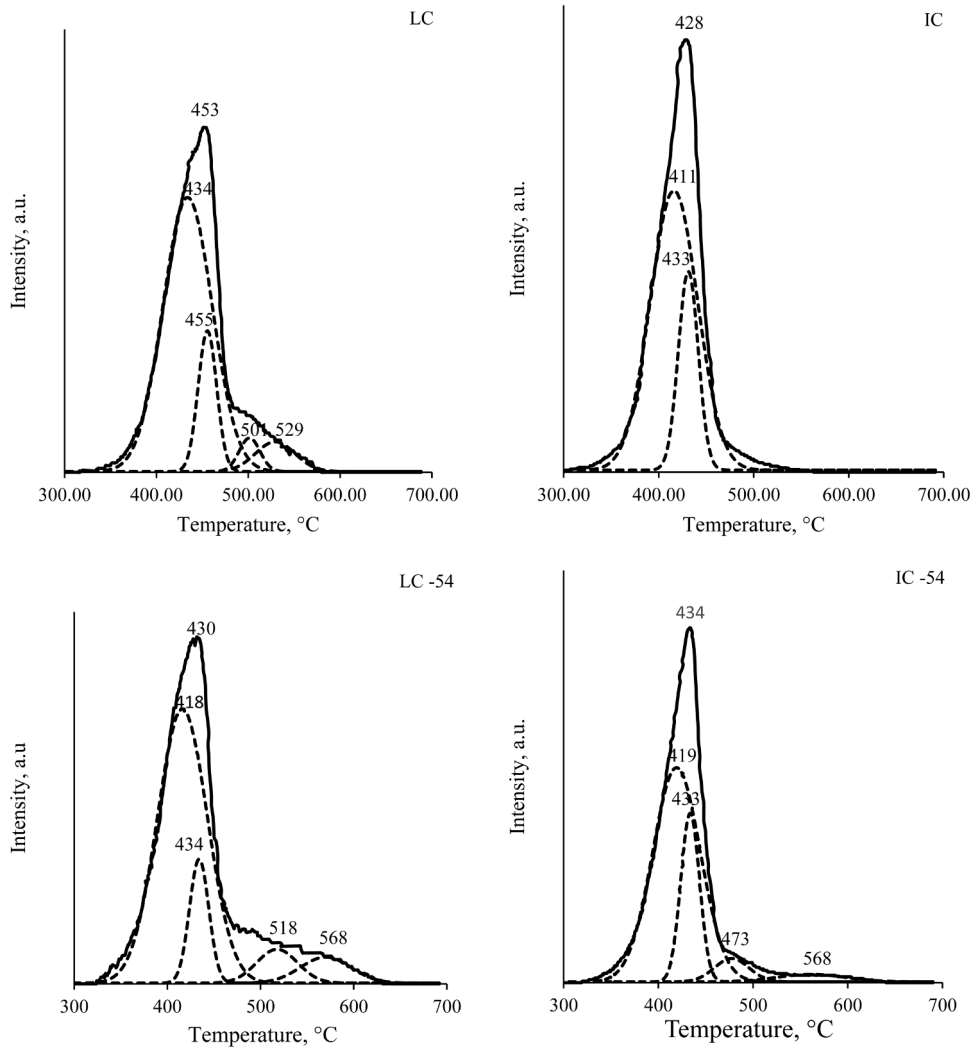

Fig. 7. H_2 TPR profiles of the reduced forms of the ChAC samples

chromates are equal to 9.9 at_{Cr}/nm^2 (Table 1). This explains the observed identical values of the initial conversion of isobutane in their presence - 56.5% by 20 minute and 57.6% by 40 minutes of the first cycle (Fig. 1). As it is known, the most active sites of ChAC in the processes of dehydrogenation of lower paraffins are chromium ions, which enter into the composition of the initial particles of amorphous Cr_2O_3 and formed in the course of the reduction of chromates.

Despite the close values of the surface concentrations of chromium due to the amorphous Cr_2O_3 and chromates at equal values of the initial conversions of isobutane, fresh laboratory and industrial ChAC provide different yields of the target products and byproducts (C_1-C_3 hydrocarbons, carbonaceous deposits) of isobutane dehydration. This indicates differences (in oxidized and reduced chromium states in samples. At a 3.5 times lower total concentration of acid sites (Table 3), laboratory ChAC provides not only a 0.39 mol iC_4H_8·Моль Cr^{-1}·h^{-1} higher specific rate of isobutylene formation with a 2-3% higher selectivity. It is also, in contrast to industrial ChAC, more stable throughout the entire test period (Fig. 1). The specific rate of isobutylene formation in the course of 54 cycles decreases by 0.09 mol iC_4H_8·Моль Cr^{-1}·h^{-1} with almost unchanged selectivity. On industrial ChAC, not only the specific rate of isobutylene formation decreases, but also the selectivity by 0.16- 0.17 mol iC_4H_8·Моль Cr^{-1}·h^{-1} и 0,3-1,0% and 0.3-1.0%, respectively.

The high activity of laboratory ChAC is related to the formation of mainly resistant to unwanted agglomeration of small particles of amorphous Cr_2O_3 and polychromates stabilized by a limited space between large crystals of α-Cr_2O_3 on its surface. According to UV-spectroscopy, only during the synthesis of the catalyst, part of Cr $(III)_{oct}$ diffuses into the crystal lattice of the alumina support. This is possible during thermal activation of the support impregnated with chromic acid. A certain amount of $Cr(III)_{oct}$ is encapsulated in fine pores of the support with a diameter of less than 5 nm. The volume of the latter is reduced by 1.5 times in comparison with the same pore volume of the support without CrO_x (Table 2). Since there are no reflections of the $(Cr_xAl_{1-x})_2O_3$ solid solution on the diffractogram of the sample (Fig. 2), it can be assumed that the content of such ions is insignificant. Therefore, it is not possible to quantify them. The bulk of chromium in the catalyst is distributed mainly in pores with a diameter of 5–20 nm, the volume of which is reduced by 0.05 cm^3/g in comparison with the support not containing CrO_x. In this case, the specific surface area decreases by 15 m^2/g. It is logical to assume that on a small (56 m^2/g) surface of the support, amorphous Cr_2O_3 particles are forced to be located between α-Cr_2O_3 crystals and/or partially on their surface. The value of the Racah parameter calculated for the chromium ion $Cr(III)_{oct}$ is 561 cm^{-1}, which is higher than the interelectron repulsion energy of the chromium ion Cr $(III)_{oct}$ in α-Cr_2O_3, equal to 441 cm^{-1}. This suggests that the size of amorphous Cr_2O_3 particles is much smaller than the size of α-Cr_2O particles. Therefore, 2.8% (m/m) of chromium participating in the formation of amorphous Cr_2O_3, with the exception of the one introduced into the support (Table 1), is structured into particles smaller than in industrial ChAC. In the latter the proportion of similar chromium is 2

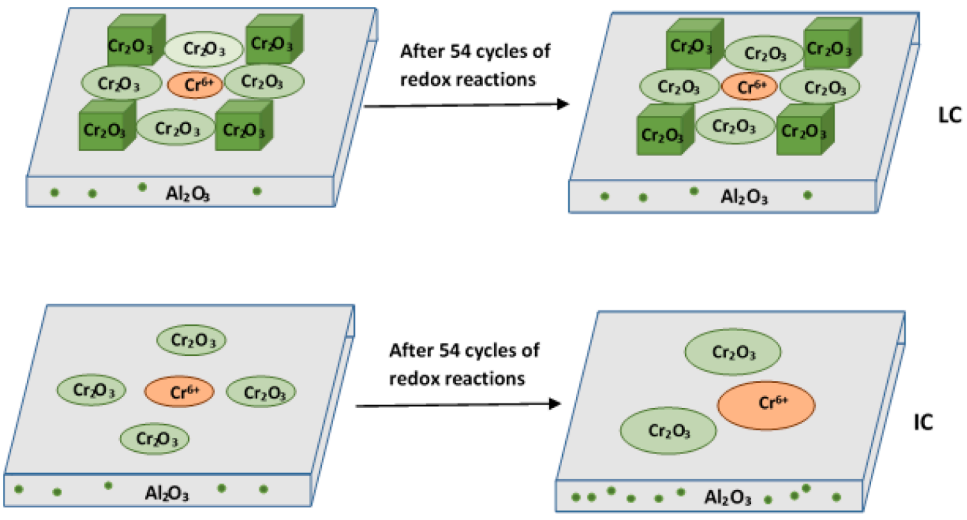

Fig. 8. Stabilization of amorphous Cr_2O_3 and polychromates particles on the γ-Al_2O_3 surface

times bigger, and the formation of large particles of amorphous Cr_2O_3 is not hindered by crystalline one. As it was shown in [20] for the example of ChAC vacuum dehydrogenation of n-butane, the activity of catalysts increases by more than 20% with a fourfold decrease in the size of amorphous Cr_2O_3 particles.

In the course of 54 cycles with an almost unchanged porous system of laboratory ChAC, the amount of α-Cr_2O_3 decreases only slightly due to the amorphization of the smallest particles. This causes a decrease in the average size of chromium particles from 582 to 570 nm. Due to polymerization of some of the monochromates, the proportion of polychromates gradually increases. The Raman spectra of reoxidized samples revealed corresponding changes in the intensities of the absorption bands caused by vibrations of Cr-O bonds in these compounds (Fig. 6). Moreover, newly formed polymerized chromates are easier to reduce than the precursors. On the TPR profiles, the effect of Cr(VI) reduction shifts to lower temperatures by 12 °C (Fig. 7). In the UV-vis spectrum of the reduced samples, polychromates are characterized by an increase in the intensities of absorption bands at 14033, 16875, and 22594 cm^{-1}. This indicates the appearance of additional redox chromium(III) in the composition of amorphous Cr_2O_3 (Figure 5). These chromium(III) ions may be additional sites of medium strength (Table 3). They enhance the surface acidity of the catalyst, but not responsible for cracking activity and coke formation. In this case, the yield of C_1-C_3 hydrocarbons does not change, while the carbon content in the catalysts, on the contrary, slightly decreases.

As a result, although the surface concentration of chromium increases to 9.8 at_{Cr}/nm^2 related to amorphous Cr_2O_3 and soluble forms of chromates (Table 2), but not related to the agglomeration of their particles (Table 1). It suggests a high resistance to migration of particles of amorphous Cr_2O_3 and polychromates on the surface of laboratory ChAC. This effect can be explained by the earlier undescribed stabilizing effect of α- Cr_2O_3 crystals. They, as is known [20], are the most stable in the course of redox cycles among all types of surface chromium oxide compounds and have low mobility on the γ-Al_2O_3 surface. The revealed stabilization of amorphous Cr_2O_3 and polychromates particles is possible with the appearance of two-phase (α-Cr_2O_3-am-Cr_2O_3 and α-Cr_2O_3-polychromate) or three-phase (polychromate-α-Cr_2O_3-am-Cr_2O_3) particles through the formation of Cr^{3+}_{cryst}-O-Cr^{3+}_{aM} and Cr^{3+}_{cryst}-O-Cr^{6+} interphase bonds (Fig. 8).

A small decrease in the conversion of isobutane (up to 56.3%) and the specific rate of isobutylene formation (up to 5.67-5.70 mol iC_4H_8·mol Cr^{-1}·h^{-1}) is related to residual after oxidizing regeneration carbonaceous deposits in pores with a diameter of 5-20 nm, screening some of the active sites. And the most difficultly reducible forms of Cr (VI) oxide compounds formed in insignificant amounts, showing on the H_2 TPR profiles of spent catalysts an additional effect at 568°C, do not have a noticeable effect on the course of side reactions. Therefore, the selectivity to isobutylene remains almost unchanged. These compounds include additional aluminum di-and tri- chromates, which are indicated by the amplification of the signal at 940 cm^{-1} in the Raman spectra (Fig. 6).

In samples of industrial ChAC, the residual carbon content is close to each other, despite the big amount of carbonaceous deposits accumulated in the course of the reaction (up to 0.6-0.7% (m/m) of carbon versus 0.4% (m/m) in laboratory ChAC). This is due to the formation of strong acidic sites with an ammonia desorption energy of more than 130 kJ/mol (Table 3). Therefore, by the 54th cycle, a decrease in the conversion of isobutane (up to 54.2-56.4%) and the specific rate of isobutylene formation (up to 5.16-5.21 mol iC_4H_8·mol Cr^{-1}·h^{-1}) is caused by the loss of a part of the highly active Cr(III) ions related to transformations in the catalyst porous system. According to UV-vis spectroscopy, chromium, which is part of the structure of polychromates, partially diffuses into the structure of the support. Which is facilitated by the disappearance of some of the pores in the range of diameters of 5-10 nm (Fig. 4), in which polychromates are likely to be encapsulated. In the Raman spectrum, the intensity of the absorption bands decreases significantly at the same time at 849 cm^{-1} due to polychromates. In addition, in the course of 54 cycles of the regeneration reactions the particles of amorphous Cr_2O_3 grow larger in the absence of the stabilizing effect of α-Cr_2O_3 crystals. The average particle diameter increases from 304 to 335 nm, which is also facilitated by a reduction in the specific surface area of the catalyst (Table 2). Monochromates partially transforming into di- and trichromates (due to them a new high-intensity absorption band appears in the Raman spectrum at 940 cm^{-1}), also form in the catalyst hardly reducible forms of chromium (VI) oxide compounds chemically bonded to the support surface. The effect of Cr(VI) reduction on the TPR profile shifts to higher temperatures by 6°C with the appearance of an additional high-temperature component, the decomposition of which into Gaussian subcomponents gives two effects at 473 and 568°C. As a result, the concentration of acid sites of medium strength and the strongest sites in the reduced forms of ChAC increases more significantly than in laboratory ChAC by 1.3 and 3.5 times, respectively (Table 3), which catalyze the side reactions of cracking and carbonization, reducing selectivity for isobutylene (Fig. 1).

Therefore, it is advisable to use an aluminum oxide support with a specific surface area of 50-60 m^2/g and a concentration of acid centers of 70 μmol NH_3/g for the synthesis of industrial microspherical ChAC. The ChAC with chromium content of ~ 7% wt. will increase the production

of isobutylene, reduce the yield of cracking products, and increase the catalyst life in the isobutane industrial dehydrogenation in the fluidized bed.

Conclusions

In this work, the stabilizing effect of α-Cr_2O_3 crystals on the highly active phases of amorphous Cr_2O_3 and polychromates was established, as well as catalytic performance of the microspherical ChAC in the process of isobutane dehydrogenation in isobutylene in a fluidized bed. It was found that with a chromium content of 7.1% (m/m) on an alumina support with a surface area of 56 m^2/g in a limited space between large crystals of α-Cr_2O_3, small particles of amorphous Cr_2O_3 and polychromates are formed. Stabilization is carried out through the formation of Cr^{3+}_{cryst}-O-Cr^{3+}_{am} and Cr^{3+}_{cryst}-O-Cr^{6+} interphase bonds in the resulting two-phase (α-Cr_2O_3-am-Cr_2O_3 and α-Cr_2O_3-polychromate) or three-phase (polychromate-α-Cr_2O_3-am-Cr_2O_3) particles, preventing from the agglomeration of amorphous Cr_2O_3 particles and polychromates in the course of redox cycles, providing with almost unchanged selectivity for isobutylene a minimum decrease in the rate of its formation. In the absence of the stabilizing effect of α-Cr_2O_3, the amorphous Cr_2O_3 particles grow larger with the migration of a part of chromium into the support and the formation of chromates with a low degree of polymerization, which more significantly reduces the rate of isobutylene formation and the catalyst selectivity.

Credit author statement

Egorova Svetlana: Writing - Original Draft, Writing - Review & Editing, Formal analysis

Tuktarov Rustem: Investigation

Boretskaya Augustina: Validation

Laskin Artem: Methodology

Gizyatullov Ramil: Visualization

Alexander Lamberov: Resources, Supervision, Project administration, Funding acquisition

Declaration of Competing Interest

The authors declare that they have no known competing financial interests or personal relationships that could have appeared to influence the work reported in this paper.

Acknowledgments

The work is performed according to the Russian Government Program of Competitive Growth of Kazan Federal University.

The phase analysis of samples was carried out at the Federal Center for Collective Use of the Kazan Federal University with the support of A. V. Gerasimov, the Russian Agency for Science and Innovation.

References

[1] D. Sanfilippo, I. Miracca, Dehydrogenation of paraffins: synergies between catalyst design and reactor engineering, Catal. Today. 111 (2006) 133–139, https://doi.org/10.1016/j.cattod.2005.10.012.

[2] Z. Nawaz, Light alkane dehydrogenation to light olefin technologies: a comprehensive review, Rev. Chem. Eng. 31 (2015) 413–436, https://doi.org/10.1515/revce-2015-0012.

[3] D. Sanfilippo, Dehydrogenations in fluidized bed: Catalysis and reactor engineering, Catal. Today. 178 (2011) 142–150, https://doi.org/10.1016/j.cattod.2011.07.013.

[4] J.J.H.B. Sattler, J. Ruiz-Martinez, E. Santillan-Jimenez, B.M. Weckhuysen, Catalytic dehydrogenation of light alkanes on metals and metal oxides, Chem. Rev. 114 (2014) 10613–10653, https://doi.org/10.1021/cr5002436.

[5] A.A. Lamberov, S.R. Egorova, K.K. Gilmanov, A.N. Kataev, G.E. Bekmukhamedov, Pilot tests of the microspherical aluminochromium KDI-M catalyst for iso-butane dehydrogenation, Catal. Ind. 9 (2017) 17–22, https://doi.org/10.1134/S2070050417010093.

[6] V.Z. Fridman, R. Xing, M. Severance, Investigating the CrO_x/Al_2O_3 dehydrogenation catalyst model: I. identification and stability evaluation of the Cr species on the fresh and equilibrated catalysts, Appl. Catal. A Gen. 523 (2016) 39–53. 10.1016/j.apcata.2016.05.008.

[7] S.R. Egorova, G.E. Bekmukhamedov, A.A. Lamberov, Effect of high-temperature treatment on the properties of an alumina-chromium catalyst for the dehydrogenation of lower paraffins, Kinet. Catal. 54 (2013) 49–58, https://doi.org/10.1134/S0023158413010072.

[8] B.M. Weckhuysen, A.A. Verberckmoes, J. Debaere, K. Ooms, I. Langhans, R. A. Schoonheydt, In situ UV–Vis diffuse reflectance spectroscopy — on lineactivity measurements of supported chromium oxide catalysts:relating isobutane dehydrogenation activity with Cr-speciationvia experimental design, J. Mol. Catal. A Chem. 151 (2000) 115–131, https://doi.org/10.1016/S1381-1169(99)00259-9.

[9] B.M. Weckhuysen, A. Bensalem, R.A. Schoonheydt, In situ UV-VIS diffuse reflectance spectroscopy-on-line activity measurements: Significance of Crn^+ species (n = 2, 3 and 6) in n-butane dehydrogenation catalyzed by supported chromium oxide catalysts, J. Chem. Soc. Faraday Trans. 94 (1998) 2011–2014, https://doi.org/10.1039/a801710g.

[10] R.L. Puurunen, B.G. Beheydt, B.M. Weckhuysen, Monitoring chromia/alumina catalysts in situ during propane dehydrogenation by optical fiber UV–Visible diffuse reflectance spectroscopy, J. Catal. 204 (2001) 253–257, https://doi.org/10.1006/jcat.2001.3372.

[11] S. Airaksinen, Chromium oxide catalysts in the dehydrogenation of alkanes, 19, Industrial Chemistry Publication Series, Espoo, 2005, pp. 1–59.

[12] A. Hakuli, M.E. Harlin, L.B. Backman, A.O.I. Krause, Dehydrogenation of i-butane on CrO_x/SiO_2 catalysts, J. Catal. 184 (1999) 349–356, https://doi.org/10.1006/jcat.1999.2468.

[13] A. Hakuli, Preparation and characterization of supported CrOx catalysts for butane dehydrogenation, Doctoral thesis, Helsinki University of Technology, Espoo, 1999, p. 48.

[14] S. De Rossi, M.P. Casaletto, G. Ferraris, A. Cimino, G. Minelli, Chromia/zirconia catalysts with Cr content exceeding the monolayer. A comparison with chromia/alumina and chromia/silica for isobutane dehydrogenation, Appl. Catal. A Gen. 167 (1998) 257–270, https://doi.org/10.1016/S0926-860X(97)00315-3.

[15] T.A. Nijhuis, S.J. Tinnemans, T. Visser, B.M. Weckhuysen, Operando spectroscopic investigation of supported metal oxidecatalysts by combined time-resolved UV-VIS/Raman/on-linemass spectrometry, Phys. Chem. Chem. Phys. 5 (2003) 4361–4365, https://doi.org/10.1039/b305786k.

[16] T.A. Nijhuis, S.J. Tinnemans, T. Visser, B.M. Weckhuysen, Towards real-time spectroscopic process control for the dehydrogenation of propane over supported chromium oxide catalysts, Chem. Eng. Sci. 59 (2004) 22–23. 10.1016/j.ces.2004.07.103.

[17] S.J. Tinnemans, M.H.F. Kox, T.A. Nijhuis, T. Visser, B.M. Weckhuysen, Real time quantitative Raman spectroscopy of supported metal oxide catalysts without the need of an internal standard, Phys. Chem. Chem. Phys. 7 (2005) 211–216, https://doi.org/10.1039/b414427a.

[18] S.J. Tinnemans, J.G. Mesu, K. Kervinen, T. Visser, T.A. Nijhuis, A.M. Beale, D. E. Keller, A.M.J. Van Der Eerden, B.M. Weckhuysen, Combining operando techniques in one spectroscopic-reaction cell: New opportunities for elucidating the active siteand related reaction mechanism in catalysis, Catal. Today. 113 (2006) 3–15. 10.1016/j.cattod.2005.11.076.

[19] V.Z. Fridman, R. Xing, Deactivation studies of the CrO_x/Al_2O_3 dehydrogenation catalysts under cyclic redox conditions, Ind. Eng. Chem. Res. 56 (2017) 7937–7947. 10.1021/acs.iecr.7b01638.

[20] V.Z. Fridman, R. Xing, Investigating the CrO_x/Al_2O_3 dehydrogenation catalyst model: II. Relative activity of the chromium species on the catalyst surface, Appl. Catal. A Gen. 530 (2017) 154–165. 10.1016/j.apcata.2016.11.024.

[21] F. Cavani, M. Koutyrev, F. Trifirò, A. Bartolini, D. Ghisletti, R. Iezzi, A. Santucci, G. Del Piero, Chemical and physical characterization of alumina-supported chromia-based catalysts and their activity in dehydrogenation of isobutane, J. Catal. 158 (1996) 236–250, https://doi.org/10.1006/jcat.1996.0023.

[22] B. Grzybowska, J. Słoczyński, R. Grabowski, K. Wcisło, A. Kozłowska, J. Stoch, J. Zieliński, Chromium oxide/alumina catalysts in oxidative dehydrogenation of isobutane, J. Catal. 178 (1998) 687–700, https://doi.org/10.1006/jcat.1998.2203.

[23] D.A. Nasimov, O.V. Klimov, A.V. Shaverina, S.V. Cherepanova, T.V. Larina, D. F. Khabibulin, A.S. Noskov, The effect of transition alumina (γ-, η-, χ-Al_2O_3) on the activity and stability of chromia/alumina catalysts. Part II: Industrial-like catalysts and real plant aging conditions, Energy Technol 7 (2019), 1800736, https://doi.org/10.1002/ente.201800736.

[24] R. Puurunen, B.M. Weckhuysen, Spectroscopic study on the irreversible deactivation of chromia/alumina dehydrogenation catalysts, J. Catal. 210 (2002) 418–430, https://doi.org/10.1006/jcat.2002.3686.

[25] S.R. Egorova, A.N. Kataev, G.E. Bekmukhamedov, A.A. Lamberov, R.R. Gil'mullin, O.N. Nesterov, Development of technology for the production of microspherical aluminum oxide supporter for the paraffin dehydrogenation catalyst, Catal. Ind. 1 (2009) 381–390, https://doi.org/10.1134/s207005040904014x.

[26] S.R. Egorova, A.N. Kataev, G.E. Bekmukhamedov, A.A. Lamberov, R.R. Gil'Mullin, O.N. Nesterov, Development of technology for the production of microspherical alumina support for the alkane dehydrogenation catalyst: II. The influence of hydrothermal treatment conditions on the operational characteristics of microspherical alumina support and chromium oxide/alumina catalyst for the dehydrogenation of iso-butane, Catal. Ind. 2 (2010) 72–86, https://doi.org/10.1134/S2070050410010125.

[27] ASTM E1941-10, ASTM Int, 2016.

[28] V.V. Yushchenko, C.J. Vanegas, B.V. Romanovskii, A method to calculate density distribution of adsorption centers from temperature-programmed desorption

spectra, Reaction Kinetics and Catalysis Letters 40 (1989) 235–240, https://doi.org/10.1007/bf02073799.
[29] C.J. Ballhausen, Introduction to Ligand Field Theory, Mac Graw-Hill Book Company, INC., 1962.
[30] B.M. Weckhuysen, L.M. De Ridder, R.A. Schoonheydt, A quantitative diffuse reflectance spectroscopy study of supported chromium catalysts, J. Phys. Chem. 97 (1993) 4756–4763, https://doi.org/10.1021/j100120a030.
[31] M.A. Vuurman, I.E. Wachs, D.J. Stufkens, A. Oskam, Characterization of chromium oxide supported on $A1_2O_3$, ZrO_2, TiO_2, and SiO_2 under dehydrated conditions, J. Mol. Catal. 80 (1993) 209–227, https://doi.org/10.1016/0304-5102(93)85079-9.
[32] M.A. Vuurman, F.D. Hardcastle, I.E. Wachs, Characterization of $CrO_3/A1_2O_3$ catalysts under ambient conditions: influence of coverage and calcination temperature, J. Mol. Catal. 84 (1993) 193–205, https://doi.org/10.1016/0304-5102(93)85052-U.
[33] L.R. Mentasty, O.F. Gorriz, L.E. Cadus, Chromium oxide supported on different Al_2O_3 supports: catalytic propane dehydrogenation, Ind. Eng. Chem. Res. 38 (1999) 396–404, https://doi.org/10.1021/ie9802562.
[34] M.A. Vuurman, D.J. Stufkens, A. Oskam, J.A. Moulijn, F. Kapteijn, Raman spectra of chromium oxide species in CrO_3/Al_2O_3 catalysts, J. Mol. Catal. 60 (1990) 83–98, https://doi.org/10.1016/0304-5102(90)85070-X.
[35] A. Oskam, D.J. Stufkens, M.A. Vuurman, Characterization of CrO_3-Al_2O_3 catalysts by Raman spectroscopy, J. Mol. Struct. 217 (1990) 325–334, https://doi.org/10.1016/0022-2860(90)80371-P.